actuators

MDPI

Article

Getting Started with PEAs-Based Flapping-Wing Mechanisms for Micro Aerial Systems

J. Carlos Durán [1,†], Juan Antonio Escareno [2,3,*,†], Gibran Etcheverry [1] and Micky Rakotondrabe [4]

1 Department of Computing, Electronics and Mechatronics, Universidad de las Américas Puebla, Sta. Catarina Mártir, San Andrés Cholula, Puebla 72810, Mexico; jose.duranhz@udlap.mx (J.C.D.); gibran.etcheverry@udlap.mx (G.E.)

2 Polytechnic Institute of Advanced Science—IPSA, IPSA's Research and Innovation Department—DRII, 15/17 rue M. Grandcoing, Ivry-sur Seine 94200, France

3 Laboratoire Informatique, Biologie Intégrative et Systémes Complexes—IBISC, 40 rue du Pelvoux, Evry 91020, France

4 Department of Control and Micro-mechatronic Systems —AS2M, FEMTO-ST Institute, University of Franche-Comté —UBFC, 25000 Besancon, France; mrakoton@femto-st.fr

* Correspondence: juan-antonio.escareno@ipsa.fr; Tel.: +33-1-56-20-62-76

† These authors contributed equally to this work.

Academic Editor: Delbert Tesar

Received: 14 December 2015; Accepted: 11 May 2016; Published: 20 May 2016

Abstract: This paper introduces recent advances on flapping-wing Micro and Nano Aerial Vehicles (MAVs and NAVs) based on Piezoelectric Actuators (PEA). Therefore, this work provides essential information to address the development of such bio-inspired aerial robots. PEA are commonly used in micro-robotics and precise positioning applications (e.g., micro-positioning and micro-manipulation), whereas within the Unmanned Aerial Vehicles (UAVs) domain, motors are the classical actuators used for rotary or fixed-wing configurations. Therefore, we consider it pertinent to provide essential information regarding the modeling and control of piezoelectric cantilever actuators to accelerate early design and development stages of aerial microrobots based on flapping-wing systems. In addition, the equations describing the aerodynamic behavior of a flapping-wing configuration are presented.

Keywords: Piezoelecric Actuators; flapping wings; MAVs; NAVs

1. Introduction

Research and Development (R&D) on aerial robotics has increased with special interest on performance improvement for MAVs and NAVs in different domains involving mechanics, control systems and robotics. The flight versatility of such vehicles has allowed us to develop a wide diversity of applications within the military and civil fields. For instance, extensive research has been conducted within the field of micro aerial robots towards aerial interactivity (aerial manipulation and grasping), swarm-based operations (sensitive or harmful zones surveillance, natural disaster assessment, convoy escort), bio-inspired configurations based tasks (zoological research, environmental observation or maritime surveillance [1]).

Concerning the size of the aerial robot; according to the Defense Advanced Research Projects Agency (DARPA) definition in the United States, a MAV features a wingspan less than 15 cm and 20 gr in mass, whereas a NAV features respectively 7.5 cm and 10 gr [2]. The development of MAVs represents a current technological trend due to the potential enhancement of current UAVs applications; for instance, search and rescue of victims after a sinister (e.g., earthquake) might be improved thanks to insect-sized robots, it grants access to locations or cavities currently unreachable

for classical mini-UAVs. Another possible application is high-resolution weather monitoring performed by a swarm of MAVs distributed throughout the zone of interest, which might be applied to air-quality monitoring (e.g., verification of polluting emission in factories) or forest fire detection. Moreover, they allow us to study the social behavior of ants or bee colonies [3]. While micro-robots featuring flapping-wing mechanisms have great promise, it also comes with significant challenges. Foremost amongst these is designing controllers that will work over the complete flight envelope of the vehicle, from near-hovering flight through to high-speed forward flight in presence of external atmospheric disturbances.

Nature has improved the bio-mechanical aerial design of insects trough millions of years of evolution. Therefore, it is logical to propose robotic aerial systems inspired by the aerial profile of insect-like flight.

In this paper, a survey over flapping-wing insect-size aerial vehicles based on Piezoelectric Actuators (PEA) is provided. The actual study has special interest on insect-like flight due to its advantageous aerial profile, offering agility and maneuverability; for instance, hovering and fast omnidirectional flight capabilities. Recent flapping mechanisms exhibit that PEA are appropriate as part of the locomotion system of such class of aerial vehicles within the micro-robotic domain due to the high resolution, high bandwidth, and high stiffness they can offer. Furthermore, their inherent property of physical reversibility makes them usable as sensors, actuators or even both at the same time. In general terms, this work intends to provide pertinent information to address the development of piezoelectric-based flapping-wing MAVs and NAVs.

2. Piezoelectric Actuators Description

Miniaturization of aerial robots changes the dynamic and structural scenario because drag becomes predominant over vehicle's weight. Size reduction also prevents the use of classical rotating motors and/or gearboxes opening the path towards PEA with cantilevered structures; they represent an interesting alternative not only for their enhanced displacement-force ratio, but also for their inverse relationship between size and actuation rate. As a consequence, PEA are used as the locomotion system of the wings controlling them in such a way that they track high-frequency oscillatory trajectories.

2.1. PEA Principle

Consider a clamped-free PEA cantilever structure as described in Figure 1a. In practice, it is composed of at least two layers. When a voltage is applied to one of the piezoelectric layers, a vertical-axis direction electrical field appears. Due to a traversal effect, this electrical field yields a contraction/expansion of the layer along the horizontal-axis. Due to the constraint between layers at their interfaces, different contraction/expansion patterns yield a deflection of the cantilever. In the sequel, we will simplify the actuator schematic with the picture in Figure 1b.

2.2. PEA Linear Modeling

When applying a sine input voltage $u(t)$ of amplitude $\hat{u}$ and frequency f to the electrodes of the piezolayers, the output deflection (displacement) δ as depicted in Figure 1c is [4]:

$$\delta(t) = \hat{u} T_1 T_2 . cos(2\pi f t) \tag{1}$$

where

$$T_1 = \frac{1}{2} \sum_{i=1}^{n} \frac{d_{31,i} w_i}{s_{11,i} h_i} \left[2\bar{z} h_i - 2h_i \sum_{j=1}^{i} h_j + h_i^2 \right] \tag{2}$$

and

$$T_2 = -\frac{4}{l^2\mu}\sum_{m=1}^{\infty} X_m \frac{k_m l \alpha_M}{\omega_m^2\sqrt{\left(1-\eta_m^2\right)^2+\left(2\varsigma_m\eta_m\right)^2}} \tag{3}$$

given l is the length of the cantilever, w is the width (supposed the same for all layers), and $\bar{z}$ is the distance of the neutral axis from the bottom surface of the cantilever. We have h_i, $d_{31,i}$ and $s_{11,i}$ as the thickness, the traversal piezoelectric constant, and the axial compliance respectively of the i-th piezoelectric layer. ω_m is the resonant frequency at mode m, X_m is the related eigenmode, and ς_m is the damping ratio. The coefficient η_m is the ratio between the excitation frequency and the m-th resonant frequency: $\eta_m = \frac{2\pi f}{\omega_m}$. Finally, $\mu = \frac{M}{l}$ is the mass to length ratio, where M is the total mass of the cantilever.

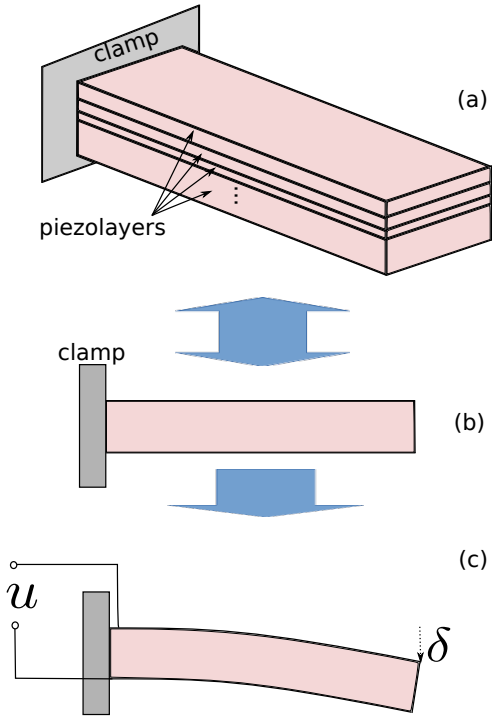

Figure 1. A piezoelecric cantilevered actuator. (**a**) Isometric scheme depicting the PEA's piezolayers; (**b**) Side view of a PEA; (**c**) bending displacement resulting as a result of the application of an input voltage u.

If the PEA is used to actuate an additional wing, the mass of the wing can be considered as well. In order to keep this review concise, we will not detail the formulas of $\bar{z}$, X_m, ς_m and the mode coefficient k_m. We encourage the reader to go to [4], where these coefficients are described in detail.

It is now understood that working at the first resonant frequency f will increase the flapping amplitude and increasing the voltage amplitude will increase this flapping range as well; therefore, voltage amplifiers are required. Another solution is to increase the number n of piezo-layers keeping the same total thickness $h = \sum_{i=1}^{n} h_i$. As each layer thickness h_i is decreased, the electrical field is higher for the same applied voltage $\hat{u}$; thus, the output displacement increases [5–7]. The adverse consequence of this proposal is the difficulty to realize multi-layer PEA and connect its electrodes for supply.

2.3. PEA Nonlinear Modeling

The previous model is linear and therefore incomplete, given PEA actuators such as those based on ceramics materials like PZT (Lead Zirconate Titanate) exhibit nonlinear behaviors like hysteresis and creep. These nonlinear characteristics drastically modify the expected PEA performance if they are not conveniently taken into account for controller synthesis.

Figure 2 depicts the hysteresis behavior between the input voltage and the output displacement of a PEA when the input is a sinusoid of amplitude 10 V at a 0.1 Hz frequency. In this example, the hysteresis amplitude is of $\frac{h}{\delta_{total}} \approx \frac{13\mu m}{88\mu m} \approx 14\%$.

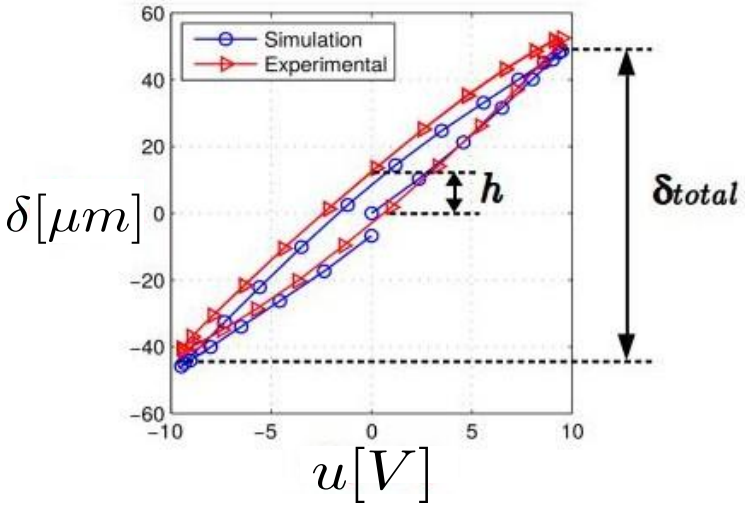

Figure 2. Curve depicting the non-linear displacement behavior of a PEA.

The PEA cantilever structure dynamic model which considers the aforementioned nonlinearities and an eventual external applied force F is as follows [5–7]:

$$\delta(s) = \Gamma_d\left(u(s), s\right) + C_r(s)u(s) + F(s)D(s) \tag{4}$$

where $\Gamma_d\left(u(s), s\right)$ is a nonlinear dynamic operator that represents the actuator's rate-dependent and dynamic hysteresis, $C_r(s)$ is a Linear-Time-Invariant (LTI) model that approximates the creep, $D(s)$ is a normalized LTI ($D(s=0)=1$), and s is the Laplace variable. Notice that the LTI approximation of the creep is important within different applications: modeling, feedforward control, feedback control and signal estimation [5–15]. $\Gamma_d\left(u(s), s\right)$ is mainly described by a rate-dependent Prandtl-Ishlinskii model [16–19]. Rate-dependent models are however, more complex to handle than rate-independent hysteresis models. Hence, the model in Equation (4) is often approximated as follows [5–8]:

$$\delta(s) = \Gamma\left(u(s)\right)D(s) + C_r(s)u(s) + F(s)D(s) \tag{5}$$

where $\Gamma\left(u(s)\right)$ is a rate-independent hysteresis model. There are several approaches used for $\Gamma\left(u(s)\right)$ in PEA, for instance: the Prandtl-Ishlinskii approach [5–7,20,21], the Preisach approach [22–24], the Bouc-Wen approach [25–28], the quadrilateral and multilinear approach [6–8,11,29]. It is noteworthy that the nonlinear model in Equations (4) and (5) come down to a linear model when the hysteresis and the creep are negligible.

2.4. PEA Control

Control of a PEA can be classified in two categories: feed-forward or open-loop control, and feedback control. The main advantage of feed-forward control is the no need of sensors yielding a

low cost and high packaging capability of the final system. There are two approaches in feed-forward control: charge control and voltage control.

Charge control consists in exploiting the linear behavior between the PEA charge and displacement [30–34] (Figure 3a). Thus, the hysteresis are lessened making control easier. However, charge control requires a well designed electrical circuit in order to provide the input charge.

Voltage control consists in finding an inverse or approximate inverse of the PEA behavior (hysteresis, creep or vibrations) and then connecting it in series with the process (Figure 3b). Many studies have been carried out regarding voltage control of hysteresis [16–20,24,25,27,28], creep [9], and of underdamped vibrations [35,36] in PEA, or their control simultaneously [10,21]. The main limitation of feed-forward control is the restricted robustness to model uncertainties and external disturbances.

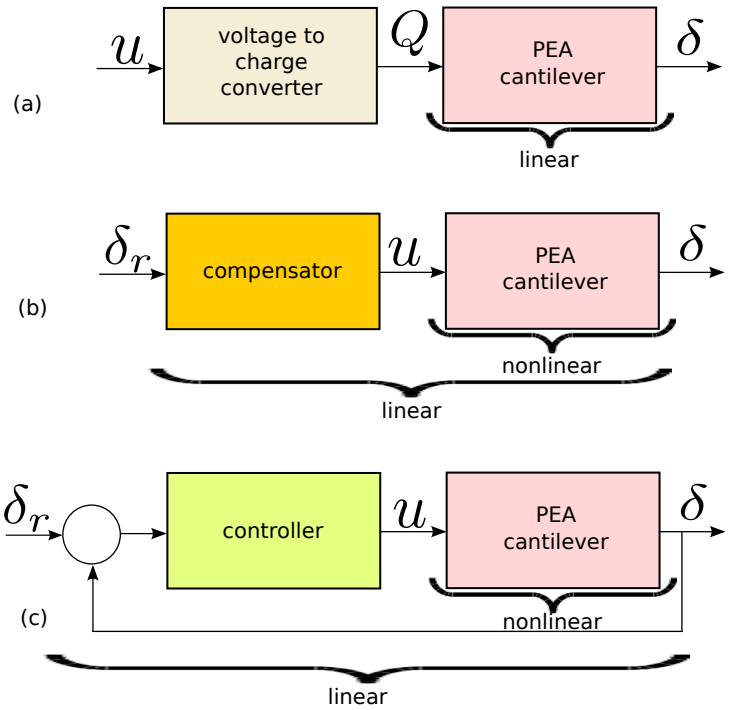

Figure 3. Displacement control of a PEA actuator. (**a**) Charge control considering that relationship of the PEA's carge and displacement are linear; (**b**) Feedfoward control structure via an hysteresis/creep compensator; (**c**) Feedback control structure based on the displacement error.

Feedback control ensures robustness and reject of eventual external disturbances by maintaining certain tracking performances (Figure 3c). However, in some applications like micro-robotics, feedback control is not always applicable because of the lack of convenient sensors to perform measurements. Many techniques have been developed to feedback control PEA based on cantilever structures, for instance: simple tuning based techniques [37–39], H_∞ based robust techniques [8,11,29,40–42], interval based robust techniques [43–45], adaptive, sliding and iterative techniques [26,46–51].

Finally, it is also possible to combine a feed-forward controller with a feedback one [52,53]. This can yield a better performance than using only one of the aforementioned control methods on their own. A complementary survey on cantilever PEA control methods are given in [5–7,54].

3. Aerodynamics of Basic Flapping-Wing Systems

Recently, significant efforts have been carried out to develop real-world operational MAVs based on flapping-wing configuration and centered towards energy efficiency during the flight.

The biomechanical generation of lift, for the avian flight, is the result of flapping the wings up (upstroke) and down (downstroke). The downstroke is the critical stage since maximal lift and thrust is produced. Whereas within upstroke stage, the wing is partially folded in order to reduce adverse aerodynamic effects as drag and negative lift forces (see Figure 4).Unlike avian flight, insects (and hummingbirds) generate the lift continuously during both backward and forward stroke. This implies that the wings are rotated to keep the leading edge in the same position and the upper and lower wings' surfaces switch positions, upper to lower and vice versa (see Figure 5).

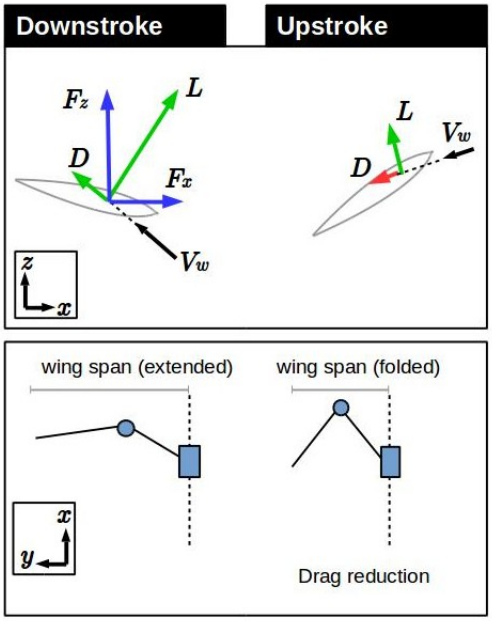

Figure 4. Avian's lift generation process.

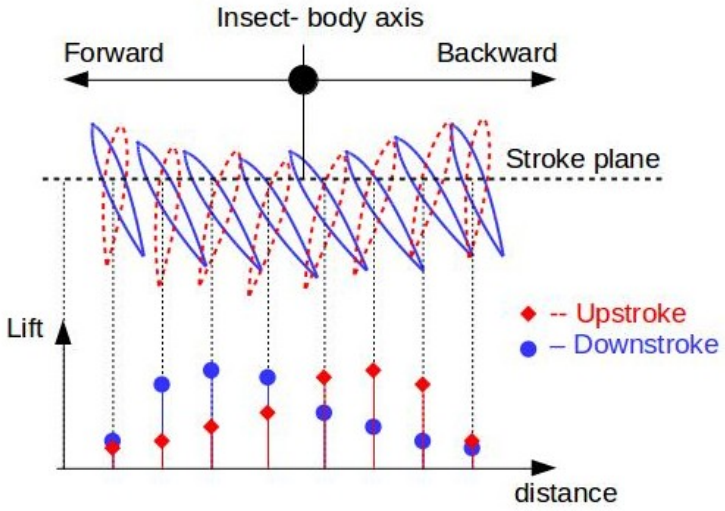

Figure 5. Insect's lift generation process.

According to [55] as a consequence of their small size, insects experience diverse adverse aerodynamic phenomena which is not present on macro-sized aerial robots. Determined by their dimensions, flying objects (airplanes, insects, birds) or even non-flying objects such as microelectromechanical systems (MEMS), are subjected to different flows and consequently to

different phenomena. The Reynolds number (R_e) indicates one of them because it is equivalent to the ratio between inertial and viscous forces contained in a fluid [56].

Dargent defined the relation of inertial and viscous forces, presented in two regimes : the viscous stokes regime (viscous forces are dominant compared to inertial forces) where $R_e < 1$, and the inertial regime where $R_e > 1$. The more an object is far from the border of viscous/inertial regimes while going towards a higher R_e, the more the turbulent phenomena will prevail over any other small scale phenomena. On other hand, the closer a flying object is to the mentioned border, the more the small scale phenomena should be considered. Given the size difference at insect scale, wing's structure and insect's weight, R_e might be completely different from one insect to another. Even for the same insect, Re is different from one flying phase to another and varies from wings to the insect's body.

Another approach is considered in the work published by Ellington [56], where he proposes an average R_e independently of the aforementioned insect structural aspects. The R_e depends on the fluid's velocity, the characteristic length and the fluid's kinematic viscosity v. In order to define an average R_e for any insect's flow regime based on the mean chord $\bar{c}$ and the average wingtip velocity $\bar{U_t}$ Ellington recommended to ignore the forward velocity; hence, we can define R_e as follows:

$$\bar{c} = \frac{2l_{wing}}{AR} \tag{6}$$

$$\bar{U_t} = 2\Phi n l_{wing} \tag{7}$$

$$R_e = \frac{\bar{U_t}\bar{c}}{v} = \frac{4\Phi n {l_{wing}}^2}{vAR} \tag{8}$$

where l_{wing} is the wing length, AR is the aspect ratio, Φ is the wingbeat amplitude(in radians) and n is the wingbeat frequency.

The first approach used by researchers to determine the insect's flight aerodynamic principles was the quasi-static approach [55]. This method assumes that instantaneous forces acting on the wings depend not only on the wing's prior motion but also on the actual motion at the instant t. Given this hypothesis, this method is normally used for objects with a high Reynolds number.

The aerodynamic force F_{aero} generated by a silhouette flow is calculated via the fluid's density ρ, the relative velocity U between the fluid and the silhouette, the wing's area S (computed by integrating $\bar{c}$ along the wing span), and the aerodynamic coefficient C_{aero} (defined by the angle of attack θ between the speed and the chord $\bar{c}$ of the silhouette):

$$F_{aero} = \frac{1}{2} C_{aero} \rho S U^2 \tag{9}$$

This approach calculates the force produced by the wings at every moment, but does not estimate the real force generated because sometimes yields forces smaller than the insect's weight, which contradicts the possibility for an insect to fly.

4. Current PEA-Based for Flapping-Wing MAVs

The Micromechanical Flying Insect (MFI) presented by researchers of University of California at Berkeley [57] was developed to accomplish maneuvering and hovering. Two piezoelectric bending actuators were used for each wing and by employing a double four bar mechanism and a differential, a rotational degree of freedom is generated to produce amplified flapping (see Figure 6. Author of [57] has granted the permission to use the pictures). These PEA are made up of PZT ceramics materials supplied with up to $\pm$200 V to produce forces of 200 mN and 400–500 µm with free displacement. Above 200 V, the actuators saturate and beyond 300 V there is a risk of electrical damage through the PZT plate.

Within another work, a 60 mg micro air vehicle using bimorph piezoelectric actuators was presented in [58]. The device consist of four mechanical components: the airframe that supplies a solid ground to the actuator and transmission; the actuator that provides motion; the transmission that amplifies the actuator motion from a translational to a rotational input, and finally the airfoils that must remain rigid to hold shape under large aerodynamic loads [59]. The device is equipped with two piezoelectric actuators so that each wing can be driven independently. The bimorph actuators were fabricated using Smart Composite Microstructure (SCM) due to their favorable scalability and compatibility with SCM process. During operation the flapping frequency is between 110–120 Hz and is able to generate torques along the three different body axes (yaw, pitch, roll). In order to achieve a sustained flight, an adaptive controller that consists in three different controllers for attitude, altitude and lateral control was implemented. The purpose of the attitude controller is to align the robot so it can maneuver in the desired direction, the lateral controller estimates the desired orientation to let the robot move to a specific position and the altitude controller computes the suitable thrust force to maintain the robot at the desired height [58]. This system has an external power supply and is able to perform successful hovering, takeoff and landing flights with these configurations with minimal error in the position accuracy.

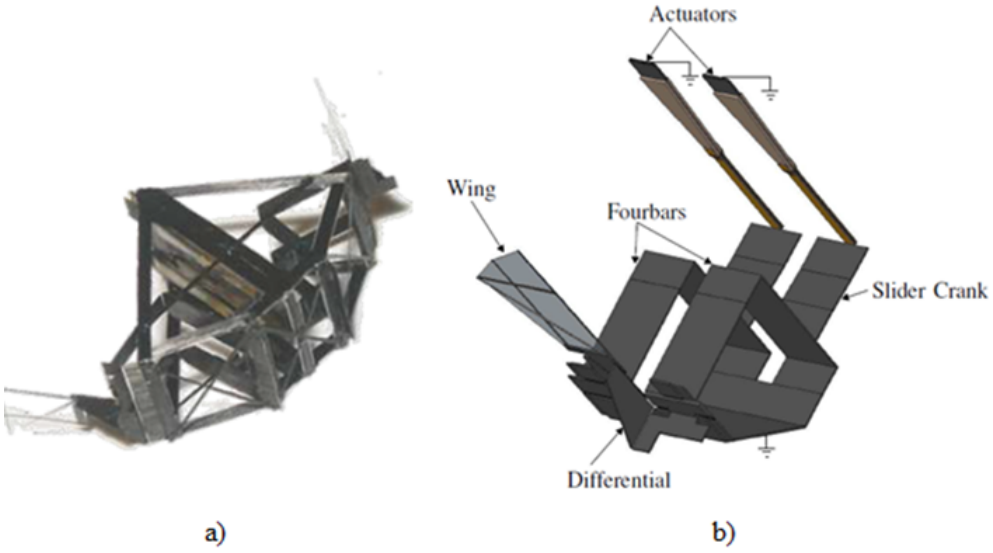

Figure 6. (**a**) Current Micromechanical Flying Insect (MFI) design (4DOF); (**b**) Flying Insect Thorax [57].

In Rahn [2], the authors focused on the design, fabrication, modeling and experimental validation of the Penn State Nano Air Vehicle (PSNAV) (see Figure 7. Author of [2] has granted the permission to use the pictures) which is a piezoelectrically actuated (it uses piezoelectric T-beam actuators) clapping wing mechanism. This mechanism amplifies the T-beam displacement through revolute joints and hinges, generating a lever mechanism that provides high movement amplification and is shifted from the horizontal plane using a small vertical offset. Hinges have to be designed to go under large deformation conditions to resist buckling when loaded.

In order to provide a large flapping and rotation angles, Rahn also introduced a process to monolithically fabricate flying insect-sized robots from SUEX dry film; this process does not use precious metals which reduces processing time and cost. With the introduction of this process they fabricated the LionFly flapping wing system powered by a piezoelectric bimorph actuator (PZT-5H) which connects separated layers of piezoelectric materials.

The PSNAV performs a 54° peak to peak wing rotation, 14° peak to peak flapping angle, and 0.21 mN thrust at 9.5 Hz, reaching a maximum thrust of 1.34 mN at 25.5 Hz. The LionFly mechanism

is able to generate a 46° flap and a 44° peak to peak rotation amplitude with relative phase of 12° and maximum lift of 71 µN at 37 Hz.

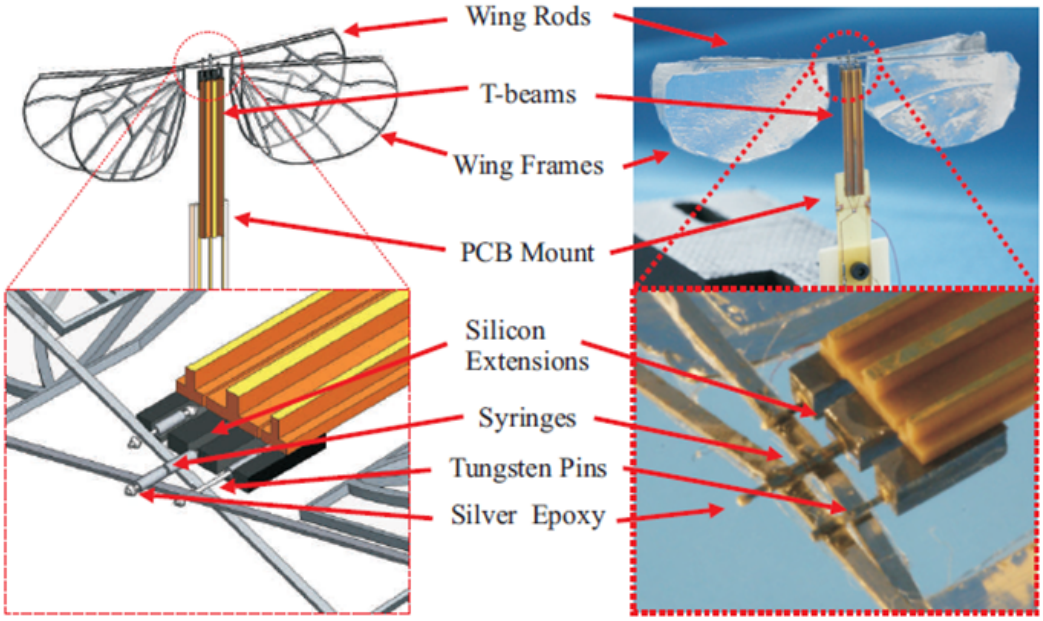

Figure 7. Conceptual design of the Penn State flapping system (**left**), four winged piezoelectric flapping system device (**right**) [2].

In [60], the authors presented a design of a simple flapping wing rotor composed of three basic elements (see Figure 8. Author of [60] has granted the permission to use the pictures): the *PEA*, the *shaft*, and the *flapping wings*. The actuator used is the *THUNDER TH-8R*, made of five layers of different materials. The wings are manufactured with four beams and each one is fabricated with two layers of carbon/epoxy laminate. This design has a lightweight configuration for the flapping wings and rotor, high aerodynamics and power efficiency, capable of performing Vertical Take-Off Landing (VTOL) and accurate maneuverability at low speed. In order to measure the total force generated by the wings, the model was fixed onto a force transducer that was also connected to a signal amplifier. The wing displacement was measured with a rotation restriction on the shaft, without considering rotational speed. The authors presented two sets of experiments: in the first one, they mounted the wing onto the actuator that was excited at a resonance frequency of 125 Hz for the flapping wing rotor to achieve maximum rotational speed and maximum dynamic force; in the second, they mesured the inertia and aerodynamic force by cutting the skin film along the dotted lines as shown in Figure 8b. In order to estimate the maximum value of aerodynamic force, the authors also performed a Computational Fluid Dynamics (CFD) simulation that agrees very good with the experimental data result. However, in relation to average aerodynamic force, the CFD showed an aerodynamic force of 3.37 mN, which is very similar to the 3.69 mN obtained in the theoretical analysis, but smaller than the 5.35 mN obtained in the experimental test; the reason for this was mainly because of the limited measurements of the wing motion and the inertia force of the second experiment performed.

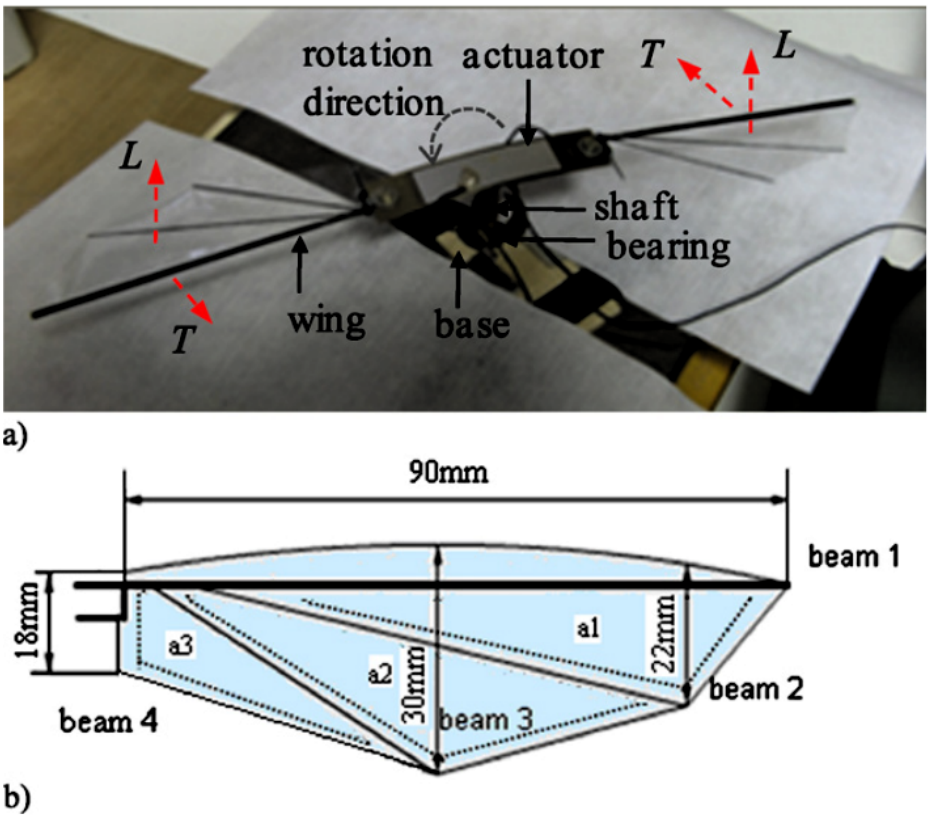

Figure 8. (**a**) The proposed configuration; (**b**) Geometric dimensions of the flapping wing [60].

In the work presented by Hall [61], in order to increase the flapping wing amplitudes, the authors created an actuator based on a layered structure using PZT segments. A Functionally Modified Bilayer (FMB) piezoelectric actuator was also fabricated to achieve 2 DOF of motion, which are the flapping motion and the bending motion. The objective of this work was to demonstrate the possibility of obtaining a flapping motion by linking a polymeric wing to a distal end of a piezoelectric bilayer actuator instead of using motors. The authors used three different types of wings for this application with the same thickness of 20 µm. The wings were based on low density polyethylene polymer (Fullcure 930), and the dimethylsiloxane electroactive polymer. Wing type 1 design presents a delay in rotation; wing type 2 does not have any batten in the span direction giving the smallest wing rotation of all designs; finally, wing type 3 has a pattern division into the number of span-wise strips that are capable of rotation independently along the longitudinal axis of the wing. During experimentation, they used a traditional bimorph actuator and the FMB actuator (both made of PZT-5H) at a flapping frequency of 21 Hz, obtaining with the former an upstroke average lift of 4 mN for wing type 1, 0 mN for wing type 2, and 2 mN for wing type 3. When using the FMB actuator with wing type 1, they obtained a lift of 10 mN thanks to the increment in flapping angle, increasing wing tip displacement and therefore, the bending moment.

Flapping systems mimics three important features of insect's flight: wing rotation, wing corrugation and wing clap. In the research presented by Nguyen *et al.* [62–64], the authors presented a flapping-wing system actuated by an unimorph piezoceramic actuator called a Lightweight Piezocomposite Actuator (LIPCA) capable of mimicking these aspects. This LIPCA is composed of five layers; three are glass/expoxy made, one more is carbon made and the last one active is PZT made [64]. The LIPCA produces a limited actuation displacement in bending mode, even if it is operating in natural frequency; for that reason, they used a four-bar linkage system to convert the limited displacement into a large flapping angle. In order to know how these aspects affect

vertical force generation, the authors performed several tests with different conditions, using two types of wings (corrugated and smooth) and with/without clap. During experimentation, the authors determined that in order to achieve largest vertical forces, they should vary the flapping frequency over a range of 5–15 Hz (Optimum Flapping Frequency). It is mentioned that wing rotation and corrugation contribute to aerodynamic force production and improvement, because the mass and flapping angle of both wings used in this work are the same. In [63] they tested the flapping wing device by using the original LIPCA and a compressed LIPCA (two carbon rods were glued to both ends). Experimentation showed that using the compressed LIPCA they improved the flapping angle (from 110° to 130°) and the vertical aerodynamic force (+24.5%). In this case, they obtained the optimum flapping frequency using two different wing shapes (horse botfly and hawk moth), where the average vertical force in both cases reached a maximum value at a flapping frequency of 9 Hz. Finally, in [64] the authors mentioned that even with small changes in wing size, aspect ratio and weight, the optimal flapping frequency is not considerably affected; for that reason, in order to increase it, a new linkage geometry is proposed. This new system is made of acrylic and the shape is taken from *hawk moth* wings (see Figure 9. Author of [64] has granted the permission to use the pictures); the size, the wing rotation angle, and the applied voltage are the same as the ones used in [62] (wings spars are made of carbon rods). These new modifications allowed the flapping system to improve 56.5% in vertical force (from 2.3 to 3.6 gF), with an optimal flapping frequency increase from 10 to 17 Hz, and a flapping angle decrease from 100° to 92°.

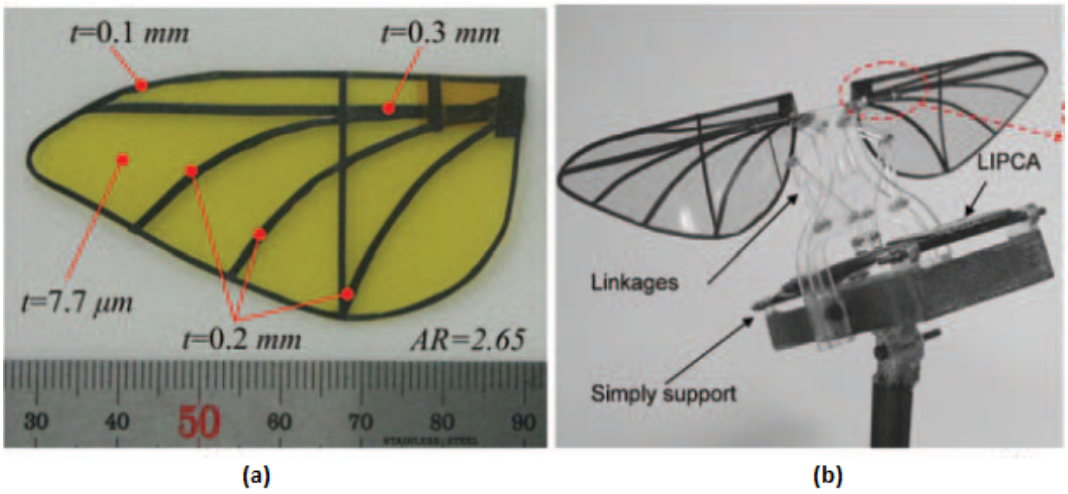

Figure 9. (**a**) Artificial Hawkmoth wing; (**b**) Fully assembled flapping system [64].

Table 1. List of main characteristics between the different prototypes of Micro Aerial Vehicles (MAVs) and Nano Air Vehicles (NAVs).

Model	Size	Actuator	Control	Beat Frequency	Lift/Thrust Generated	Other Features
[57]	25 mm (wingtip to wingtip)	Unimorph piezoelectric bending actuators	Feedback Control	275 Hz	L: 1400 µN	Piezoelectric actuator stiffness 400 N/m.
[58]	30 mm wingspan	Bimorph piezoelectric clamped-free bending cantilever	Adaptive Control	120 Hz	T > 1.3 mN	80 mg FW using Smart Composite Microstructures (SCM) process
[2]	37.5 mm wingspan	Piezoelectric T-beams	-	25.5 Hz	T: 1.34 mN	-
[60]	90 mm wingspan	Piezoelectric THUNDER TH-8R	-	125 Hz	L: 5.35 mN	-
[61]	-	Bimorph Piezoelectric and a Functionally Modified Bimorph (FMB)	-	21 Hz	L: 10 mN	Flapping angle of 45°
[62–64]	-	Unimorph Piezoceramic, Lightweight Piezocomposite actuator (LIPCA)	-	17 Hz	-	Flapping angle of 92°

5. Concluding Remarks and Open Questions

We presented in this paper the use of cantilever PEA as potential actuators in MAVs based on flapping mechanisms. The focus of the paper is to provide essential information while addressing the development of flapping-wing-based aerial robots at earlier stages, especially for those UAVs research groups whose expertise does not entail PEAs modeling and control. Structural and operational advantages mentioned above allow small wings to flap with high amplitude at high frequencies. Figure 10 depicts a basic version of the "Piezowing" currently under development.

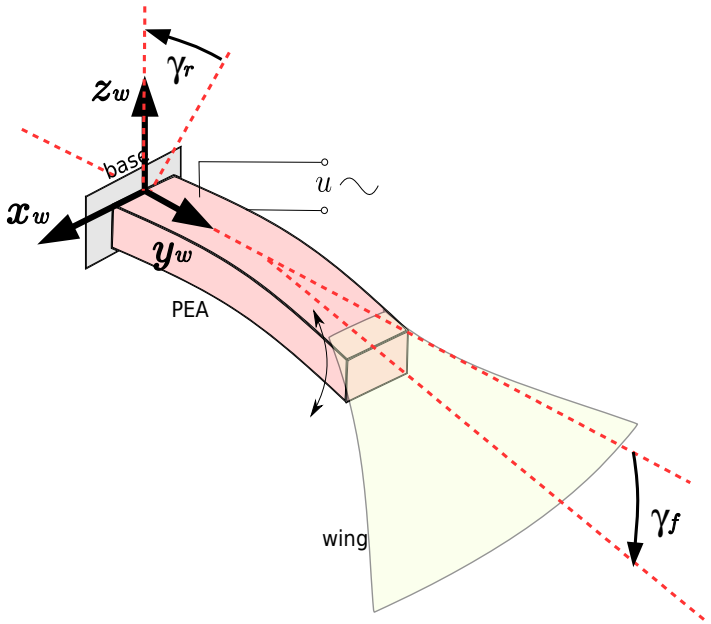

Figure 10. Perspective Piezowing: the PEA actuates directly to flap microrobot's wing. The flapping angle and wing's lift attitude respectively stand for γ_f and γ_r. The latter angle is generated by a PEA-based joint located at Piezowing's base.

PEAs are well known for their high bandwidth and compactness, which are convenient properties for flapping-wing MAVs. We presented the PEA operational principles and then reviewed their linear and nonlinear models. The control strategies employed for these devices mainly come from nano-positioning applications, but they can serve as a starting point to control PEA based flapping-wing MAVs. Structural and operational advantages mentioned above allow small wings to flap with high amplitude at high frequencies. Figure 10 depicts a basic version of the "Piezowing" currently under development.

The herein presented study shows this is a young field of research with questions to be explored in more detail. For instance, the fabrication process and the assembly of the 3D structures for MAVs is a challenging work as their sizes decrease. A new and highly evolving technology that can be used to realize such miniaturized MAV is 3D printing and additive manufacturing. It was shown that this technology could be very promising for the development of complex miniaturized system based on piezoelectric actuators [65,66]. The design itself of the piezoelecric actuators can also be optimized in order to ensure the performances of the MAV. For instance, in [67,68], two methodologies of design for piezoelectric cantilever actuators that should satisfy some predefined performances with minimization of the dimensions have been suggested on the basis of the interval techniques and control theory tools combined and developed in [69]. FInally, powering the piezoelectric actuators is still a great challenge. Indeed, such actuators often require high voltage (but low current), sometimes up to tens of or more than a hundred Volts. However, endeavor in recent promising researches [70,71] dealt to develop novel piezoactuators with low voltages

functioning. Called thick-films technology, the principle is to thin the thick layers of the PZT piezoelectric actuators, and thus with low voltage, high electric field is obtained and consequently large deformation/displacement is obtained. Performed in clean-room, another advantage of this PZT thinning technique is the high miniaturization aspect: down to tens of µm of thicknesses and length of some millimeters of the PZT cantilever actuator can be realized. A very interesting feature could therefore be to combine embedded piezoelectric energy harvester with a convenient power generator to supply the low voltages thin piezoelectric cantilever actuators.

All these questions are non exhaustive and pose great challenges in order to develop high performance and high energy-autonomy MAVs.

Aknowledgments: This work is supported by the national ANR-JCJC C- MUMS-project (National young investigator project ANR-12- JS03007.01: Control of Multivariable Piezoelectric Microsystems with Minimization of Sensors). This work is also supported by the LABEX ACTION.

Author Contributions: J. Carlos Durán and Juan Antonio Escareno have contributed equitably, focusing on state of the art, aerodynamics (equations and schemes) and control techniques applied to PEAs. Whereas Gibran Etcheverry and Micky Rakotondrabe has provided the detailed description and schemes of PEAs. Micky Rakotondrabe has contributed with valuable corrections and comments to the submitted versions regarding the overall organization of the paper.

Conflicts of Interest: The authors declare no conflict of interest.

References

1. Eisenbeiss, H. A Mini Unmanned Aerial Vehicle (UAV): System overview and image acquisition. In Proceedings of the International Workshop on Processing and Visualization Using High-Resolution Imagery, Pitsanulok, Thailand, 18–20 November 2004.
2. Rahn, C.; Tadigadapa, S. *High Performance Piezoelectric Actuators and Wings for Nano Air Vehicles (NAVs)*; Pennsylvania State University: State College, PA, USA, 2012.
3. Wood, R.; Nagpal, R.; Wei, G.Y. Flight of the Robobees. Available online: http://www.scientificamerican.com/article/robobee-project-building-flying-robots-insect-size/ (accessed on 12 May 2016).
4. Ballas, R.G. *Piezoelectric Multilayer Beam Bending Actuators: Static and Dynamic Behavior and Aspects of Sensor Integration*; Springer: Berlin, Germany, 2007.
5. Rakotondrabe, M. *Piezoelectric Cantilevered Structures: Modeling Control and Measurement/Estimation Aspects*; Springer-Verlag: Berlin, Germany, Monography in preparation.
6. Rakotondrabe, M. *Smart Materials-Based Actuators at the Micro/Nano-Scale: Characterization, Control and Applications*; Springer-Verlag: New York, NY, USA, 2013.
7. Rakotondrabe, M. Piezoelectric Systems for Precise and High Dynamic Positioning: Design, Modeling, Estimation and Control. "Habilitation à diriger la recherche (HDR)" Dissertation, University of Franche-Comté/FEMTO-ST, Besançon, France, 2014.
8. Rakotondrabe, M.; Haddab, Y.; Lutz, P. Quadrilateral modelling and robust control of a nonlinear piezoelectric cantilever. *IEEE Trans. Control Syst. Technol.* **2009**, *17*, pp. 528–539.
9. Rakotondrabe, M. Modeling and Compensation of Multivariable Creep in multi-DOF Piezoelectric Actuators. In Proceedings of the IEEE International Conference on Robotics and Automation, St. Paul, MN, USA, 14 May 2012; pp. 4577–4581.
10. Croft, D.; Shed, G.; Devasia, S. Creep, hysteresis and vibration compensation for piezoactuators: Atomic force microscopy application. *ASME J. Dynamic Syst. Meas. Control* **2001**, *123*, pp. 35–43.
11. Habineza, D.; Rakotondrabe, M.; Le Gorrec, Y. Characterization, Modeling and H-inf Control of n-DOF Piezoelectric Actuators: Application to a 3-DOF Precise Positioner. *Asian J. Control* **2016**, *18*, pp. 1–20.
12. Rakotondrabe, M. Combining self-sensing with an Unkown-Input-Observer to estimate the displacement, the force and the state in piezoelectric cantilevered actuator. In Proceedings of the American Control Conference, Washington, DC, USA, 18 June 2013; pp. 4523–4530.
13. Trenchant, V.; Rakotondrabe, M.; Haddab, Y. Force estimation in a 2-DOF piezoelectric actuator by using the inverse-dynamics based unknown input observer technique. *Proc. SPIE* **2015**, *9494*, doi:10.1117/12.2185682.

14. Rakotondrabe, M.; Lutz, P. Force estimation in a piezoelectric cantilever using the inverse-dynamics-based UIO technique. In Proceedings of the IEEE International Conference on Robotics and Automation, Kobe, Japan, 12–17 May 2009; pp. 2205–2210.
15. Rakotondrabe, M.; Haddab, Y.; Lutz, P. Nonlinear modelling and estimation of force in a piezoelectric cantilever. In Proceedings of the IEEE/ASME International Conference on Advanced Intelligent Mechatronics, Zurich, Switzerland, 5 September 2007.
16. Aljanaideh, O.; Habineza, D.; Rakotondrabe, M.; Al Janaideh, M. Experimental comparison of rate-dependent hysteresis models in characterizing and compensating hysteresis of piezoelectric tube actuators. *Phys. B Condens. Matter* **2015**, doi:10.1016/j.physb.2015.10.021.
17. Aljanaideh, O.; Al Janaideh, M.; Rakotondrabe, M. Enhancement of Micro-positioning Accuracy of a Piezoelectric Positioner by Suppressing the Rate-Dependant Hysteresis Nonlinearities. In Proceedings of the IEEE/ASME International Conference on Advanced Intelligent Mechatronics, Besançon, France, 10 July 2014; pp. 1683–1688.
18. Ang, W.; Kholsa; P.; Riviere, C. Feedforward controller with inverse rate-dependent model for piezoelectric actuators in trajectory-tracking applications. *IEEE/ASME Trans. Mechatron.* **2007**, *12*, 134–142.
19. Al Janaideh, M.; Krejci, P. Inverse rate-dependent prandtl-ishlinskii model for feedforward compensation of hysteresis in a piezomicropositioning actuator. *IEEE/ASME Trans. Mechatron.* **2013**, *18*, 1498–1507.
20. Rakotondrabe, M. Classical Prandtl-Ishlinskii modeling and inverse multiplicative structure to compensate hysteresis in piezoactuators. In Proceedings of the American Control Conference, Montréal, QC, Canada, 27 June 2012; pp. 1646–1651.
21. Rakotondrabe, M.; Clevy, C.; Lutz, P. Complete open loop control of hysteretic, creeped, and oscillating piezoelectric cantilevers. *IEEE Trans. Autom. Sci. Eng.* **2010**, *7*, 440–450.
22. Hughes, D.; Wen, J.T. Preisach modeling of piezoceramic and shape memory alloy hysteresis. *Smart Mater. Struct.* **1997**, *4*, 287–399.
23. Dubra, A.; Massa, J.; Paterson, C. Preisach classical and nonlinear modeling of hysteresis in piezoceramic deformable mirrors. *Opt. Express* **2005**, *13*, 9062–9070.
24. Oubellil, R.; Ryba, L.; Voda, A.; Rakotondrabe, M. Experimental model inverse-based hysteresis compensation on a piezoelectric actuator. In Proceedings of the IEEE International Conference on System Theory, Control and Computing, Cheile Gradistei-Fundata Resort, Galati, Romania, 14 October 2015; pp. 186–191.
25. Rakotondrabe, M. Bouc-Wen modeling and inverse multiplicative structure to compensate hysteresis nonlinearity in piezoelectric actuators. *IEEE Trans. Autom. Sci. Eng.* **2011**, *8*, 428–431.
26. Escareno, J.; Rakotondrabe, M.; Habineza, D. Backstepping-based robust-adaptive control of a nonlinear 2-DOF piezoactuator. *IFAC Control Eng. Pract.* **2015**, *41*, 57–71.
27. Habineza, D.; Rakotondrabe, M.; Le Gorrec, Y. Bouc-Wen Modeling and Feedforward Control of multivariable Hysteresis in Piezoelectric Systems: Application to a 3-DoF Piezotube scanner. *IEEE Trans. Control Syst. Technol.* **2015**, *23*, 1797–1806.
28. Habineza, D.; Rakotondrabe, M.; Le Gorrec, Y. Multivariable generalized Bouc-Wen modeling, identification and feedforward control and its application to a 2-DoF piezoelectric multimorph actuator. In Proceedings of the IFAC World Congress, Cape Town, South Africa, 29 August 2014; pp. 10952–10958.
29. Rakotondrabe, M.; Haddab, Y.; Lutz, P. Plurilinear modeling and discrete μ-synthesis control of a hysteretic and creeped unimorph piezoelectric cantilever. In Proceedings of the IEEE International Conference on Automation, Robotics, Control and Vision, Grand Hyatt, Singapore, 5 December 2006; pp. 57–64.
30. Comstock, R.H. Charge Control Actuators to Reduce Hysteresis Effects. U.S. Patent No. 4,263,527, 21 April 1981.
31. Newcomb, C.V.; Flinn, L. Improving the linearity of piezoelectric actuators. *J. Electron. Lett.* **1982**, *18*, 442–443.
32. Newton, D.; Main, J.; Garcia, E. Piezoelectric actuation systems: Optimisation of driving electronics. *Proc. SPIE* **1996**, *2717*, doi:10.1117/12.239029.
33. Agnus, J.; Chaillet, N. Dispositif de commande d'un actionneur piezoelectrique et scanner muni de ceux-ci. INPI Patent No. N FR20030000532, 23 July 2004. (In French)
34. Rios, S.; Fleming, A.J. Control of Piezoelectric Benders Using a Charge Drive. In Proceedings of the International Conference on New Actuators, Bremen, Germany, 23 June 2014.

35. Habineza, D.; Rakotondrabe, M.; Le Gorrec, Y. Simultaneous Suppression of Badly-Damped Vibrations and Cross-couplings in a 2-DoF piezoelectric actuator, by using Feedforward Standard H-inf approach. *Proc. SPIE* **2015**, *9494*, doi:10.1117/12.2192746.
36. Al Hamidi, Y.; Rakotondrabe, M. Multi-Mode Vibration Suppression in 2-DOF Piezoelectric Systems Using Zero Placement Input Shaping Technique. *Proc. SPIE* **2015**, *9494*, doi:10.1117/12.2185683.
37. Choi, G.S.; Kim, H.-S.; Choi, G.H. A study on position control of piezoelectric actuators. In Proceedings of the IEEE International Symposium on Industrial Electronics, Guimaraes, Portugal, 7–11 July 1997; pp. 851–855.
38. Kenton, B.J.; Leang, K.K. Design and Control of a Three-Axis Serial Kinematic High-Bandwidth Nanopositioner. *IEEE/ASME Trans. Mechatron.* **2012**, *17*, pp. 356–369.
39. Soltani Bozchalooi, I.; Youcef-Toumi, K. Multi-actuation and PI control: A simple recipe for high-speed and large-range atomic force microscopy. *Ultramicroscopy* **2014**, *146*, 117–124.
40. Mahmood, I.A. ; Liu, K.; Moheimani, S.O.R. Two Sensor Based H-Infinity Control of a Piezoelectric Tube Scanner. In Proceedings of the IFAC World Congress, Seoul, Korea, 6–11 July 2008.
41. Daniele, A.; Salapaka, S.; Salapaka, M.V.; Dahleh, M. Piezoelectric scanners for atomic force microscopes: Design of lateral sensors, identification and control. In Proceedings of the American Control Conference, San Diego, CA, USA, 2–4 June 1999; Volume 1, pp. 253–257.
42. Chibum, L.; Salapaka, S.M. Robust broadband nanopositioning: Fundamental trade-offs, analysis, and design in a two-degree-of-freedom control framework. *Nanotechnology* **2009**, *20*, 035501.
43. Khadraoui, S.; Rakotondrabe, M.; Lutz, P. Interval Modeling and Robust Control of Piezoelectric Microactuators. *IEEE Trans. Control Sys. Technol.* **2012**, *20*, 486–494.
44. Khadraoui, S.; Rakotondrabe, M.; Lutz, P. Combining H-inf approach and interval tools to design a low order and robust controller for systems with parametric uncertainties: Application to piezoelectric actuators. *Int. J. Control* **2012**, *85*, 251–259.
45. Khadraoui, S.; Rakotondrabe, M.; Lutz, P. Design of RST-structured controller for parametric uncertain system using interval analysis: Application to piezocantilever. *Asian J. Control* **2013**, *15*, 142–154.
46. Xu, Q.; Li, Y., Global sliding mode-based tracking control of a piezo-driven xy micropositioning stage with unmodeled hysteresis. In Proceedings of the IEEE/RSJ International Conference on Intelligent Robots and Systems, St. Louis, MO, USA, 15 November 2009.
47. Yu, S.; Shirinzadeh, B.; Alici, G.; Smith, J. Sliding mode control of a piezoelectric actuator with neural network compensating rate-dependent hysteresis. In Proceedings of the IEEE International Conference on Robotics and Automation, Barcelona, Spain, 18–22 April 2005; pp. 3641–3645.
48. Chen, X.; Hisayama, T. Adaptive sliding-mode position control for piezo-actuated stage. *IEEE Trans. Ind. Electron.* **2008**, *55*, 3927–3934.
49. Liaw, H.C.; Shirinzadeh, B.; Smith, J. Enhanced sliding mode motion tracking control of piezoelectric actuators. *Sens. Actuators A Phys.* **2007**, *138*, 194–202.
50. Sofla, M.S.; Rezaei, S.M.; Zareinejad, M.; Saadat, M. Hysteresis-observer based robust tracking control of piezoelectric actuators. In Proceedings of the American Control Conference, Baltimore, MD, USA, 30 June–2 July 2010; pp. 4187–4192.
51. Tien, S.; Zou, Q.; Devasia, S. Iterative control of dynamics-coupling-caused errors in piezoscanners during high-speed AFM operations. *IEEE Trans. Control Syst. Technol.* **2005**, *13*, 921–931.
52. Rakotondrabe, M.; Rabenorosoa, K.; Agnus, J.; Chaillet, N. Robust feedforward-feedback control of a nonlinear and oscillating 2-dof piezocantilever. *IEEE Trans. Autom. Sci. Eng.* **2011**, *8*, 506–519.
53. Rakotondrabe, M.; Al Janaideh, O.; Al Janaideh, M. H-inf Control for a Smart Micro-Positioning System with an Analytical Model for the Output of the Inverse Compensation. In Proceedings of the American Control Conference, Chicago, IL, USA, 1–3 July 2015; pp. 2643–2648.
54. Devasia, S.; Eleftheriou, E.E.; Moheimani, R. A survey of control issues in nanopositioning. *IEEE Trans. Control Syst. Technol.* **2007**, *15*, 802–823.
55. Dargent, T. Microsystème à ailes vibrantes: Utilisation des technologies MEMS pour la réalisation d'un microdrone bioinspiré. Ph.D. Thesis, Université de Valenciennes et du Hainaut-Cambresis, Famars, France, 2011. (Thesis In French)
56. Ellington, C. The novel aerodynamics of insect flight: Applications to microair vehicles. *J. Exp. Biol.* **1999**, *202*, 3439–3448.

57. Steltz, E.; Avadhanuka, S.; Fearing, R. High lift force with 275 Hz wing beat in MFI. In Proceedings of the International Conference on Intelligent Robots and Systems, San Diego, CA, USA, 29 October–2 November 2007; pp. 3987–3992.
58. Chirarattananon, P.; Ma, K.Y.; Wood, R. Adaptive control for takeoff, hovering, and landing of a robotic fly. In Proceedings of the International Conference on Intelligent Robots and Systems, Tokyo, Japan, 3–7 November 2013.
59. Wood, R. The first takeoff of a biologically inspired at-scale robotic insect. *IEEE Trans. Robot.* **2008**, *24*, 341–347.
60. Guo, S.; Li, D.; Wu, J. Theoretical and experimental study of a piezoelectric flapping wing rotor for micro aerial vehicle. *Aerosp. Sci. Technol.* **2011**, *23*, 429–438.
61. Hall, A.; Roberts, R.; Weintraub, I.; Riddick, J. *Flapping Wing Technology for Micro Air Vehicles Incorporating a Lead Zirconate Titanate (PZT) Bimorph Actuator*; U.S. Army Research Laboratory: Adelphi, MD, USA, 2012.
62. Nguyen, Q.; Syaifuddin, M.; Park, H.; Byun, D.; Goo, N.; Yoon, K. Characteristics of an Insect-mimicking Flapping System Actuated by a Unimorph Piezoceramic Actuator. *J. Intell. Mater. Syst. Struct.* **2008**, *19*, 1185–1193.
63. Nguyen, Q.; Park, H.; Goo, N.; Byun, D. Aerodynamic force generation of an insect-inspired flapper actuated by a compressed unimorph actuator. *Chin. Sci. Bull.* **2009**, *54*, 2871–2879.
64. Truong, Q.; Nguyen, Q.; Park, H.; Byun, D.; Goo, N. Modification of a Four-Bar Linkage System for a Higher Optimal Flapping Frequency. *J. Intell. Mater. Syst. Struct.* **2011**, *22*, 59–66.
65. Gendreau, D.; Rougeot, P.; Mohand-Ousaid, A.; Rakotondrabe, M. 3D-Printing: A promising technology to design three-dimensional microsystems. In Proceedings of the International Conference on Manipulation, Automation and Robotics at Small Scales, Paris, France, 18–22 July 2016.
66. Mohand-Ousaid, A.; Gendreau, D.; Rougeot, P.; Rakotondrabe, M. Design, static modeling and simulation of a 5-DOF precise piezoelectric positioner. In Proceedings of the SPIE Sensing Technology + Applications: Sensors for Next Generation Robots Conference, Baltimore, MD, USA, 21 April 2016.
67. Khadraoui, S.; Rakotondrabe, M.; Lutz, P. Optimal design of piezoelectric cantilevered actuators with guaranteed performances by using interval techniques. *IEEE/ASME Trans. Mechatron.* **2014**, *19*, 1660–1668.
68. Rakotondrabe, M.; Khadraoui, S. Design of Piezoelectric Actuators with Guaranteed Performances using the Performances Inclusion Theorem and Interval Tools. In *Smart Materials-Based Actuators at the Micro/Nano-Scale: Characterization, Control and Applications*; Rakotondrabe, M., Ed.; Springer-Verlag: New York, NY, USA, 2013.
69. Rakotondrabe, M. Performances inclusion for stable interval systems. In Proceedings of the American Control Conference, San Francisco, CA, USA, 30 June 2011; pp. 4367-4372.
70. Bienaime, A.; Chalvet, V.; Clevy, C.; Gauthier-Manuel, L.; Baron, T.; Rakotondrabe, M. Static/dynamic trade-off performance of PZT thickfilm micro-actuators. *J. Micromech. Microeng.* **2015**, *25*, 075017.
71. Chalvet, V.; Habineza, D.; Rakotondrabe, M.; Clevy, C. Hysteresis characterization of novel thick-film PZT microactuators. *Phys. B Condens. Matter* **2015**, doi:10.1016/j.physb.2015.11.007.